7
Photo-Response of Flexible OFETs

One of the very widely explored applications of high performance organic and inorganic devices is sensing. Organic semiconductors are highly sensitive to external physical stimuli like pressure, gas, environment and light. Use of OFETs for sensing has also been viable with extended chemical and biological sensing capabilities. In addition, third main aim of the research work undertaken was to use high performance OFETs in sensing applications. Keeping this objective under purview, flexible OFETs with an active layer of neat TIPS-pentacene have been explored as photo-transistors, and the findings of the same are discussed in this chapter. Photo-response of these flexible OFETs has been evaluated under illumination of visible light of different colors and ultra-violet light.

7.1 INTRODUCTION

Advantages of low cost and simplicity have led to the successful integration of OFETs in low cost and efficient detection devices also, with wide range of functionality including chemical sensing [Feng *et al.*, 2016], bio-sensing [Sokolov *et al.*, 2009], gas sensing [Zhang *et al.*, 2015], and pressure sensing [Lai *et al.*, 2013]. In addition, OFETs have been incorporated in several optical devices such as light sensors [Huang *et al.*, 2014, Kim *et al.*, 2010, Liu *et al.*, 2016], photo-controlled switches and optoelectronic memory elements [Ji *et al.*, 2010, Zhan *et al.*, 2011, Baeg *et al.*, 2012], due to photo-sensitive properties of organic semiconductors. An optical FET or a photo-FET is superior to photo diode due to its combined ability of light detection and amplification along with higher responsivity. Therefore, photo-OFETs have been explored with great interest with various device geometries and materials [Dutta and Narayan, 2003, Dutta *et al.*, 2004, Dutta and Narayan, 2005, Joshi *et al.*, 2014]. Several organic semiconductors, both small molecules like Pentacene [Nickel, 2009], and polymeric like dinaphtho[2,3-b:2′,3′-f]thieno[3,2-b]thiophene (DNTT) [Milvich *et al.*, 2015], N,N′-ditridecyl-3,4,9,10-perylenetetracarboxylic diimide (PTCDI-$C_{13}H_{27}$) [Chou *et al.*, 2014], 6,13-bis(triisopropylsilylethynyl) pentacene (TIPS-pentacene) [Kim *et al.*, 2010, Jae-Hong *et al.*, 2009], and Poly(3-hexylthiophene-2,5-diyl) (P3HT) [Dutta and Narayan, 2004] have been efficiently deployed in photo-OFETs. Most of these photo-OFETs are either demonstrated on rigid substrates or their operating voltages are high. Hence, demonstration of low voltage and high performance photo-OFETs on flexible platforms is essential for large area electronics applications.

In addition, majority of reports deal with photo-sensitive properties of organic semiconductors in the visible range of electromagnetic spectrum. Effect of ultra-violet (UV) irradiation on organic semiconductors largely remains under-explored with very less reports available. Nonetheless, development of low cost, low power and high performance UV detectors based on organic semiconductors is highly imperative for several civil and military applications including smoke and fire detection, missile warning, combustion monitoring and ozone sensing [Monroy *et al.*, 2003, Razeghi and Rogalski, 1996]. For most of the organic semiconductors, which have been explored as UV detectors, corresponding devices are in the diode architecture and have been fabricated on rigid substrates [Li *et al.*, 2005, Chen *et al.*, 2006, Si *et al.*, 2007, Ray and Narasimhan, 2007, Zhang *et al.*, 2010, Li *et al.*, 2011]. However as discussed before, a photo-OFET is always a better choice over a photo-diode due to

simultaneous photo-detection and amplification along with higher sensitivity. Despite this fact, reports on UV detectors based on OFETs are unfortunately obscure and effect of UV irradiation on the performance of OFETs remain under-addressed. For this reason, it is highly essential to study the effect of UV irradiation on the electrical characteristics of OFETs.

In this chapter, solution processed photo-OFETs fabricated on flexible substrates have been demonstrated with neat TIPS-pentacene as the photo-sensitive active layer. The second device strategy (active layer of neat TIPS-pentacene on HfO_2-PVP bi-layer gate dielectric) explored in chapter 5, has been selected to study the photo-response of TIPS-pentacene OFETs due to relatively simpler device structure and of larger content of TIPS-pentacene in the active layer than their PS blend counterparts. Photo-OFETs function at moderate operating voltage of -10 V. Pristine OFETs show an average mobility of 0.11±0.08 $cm^2 V^{-1} s^{-1}$ with maximum of 0.23 $cm^2 V^{-1} s^{-1}$ with high current on-off ratio of 10^5. Photo-response of the devices was measured under irradiation of visible light of different colors ($\lambda_{min,r}$ = 620 nm; red, $\lambda_{min,g}$ = 520 nm; green and $\lambda_{min,b}$ = 460 nm; blue light). Photo-OFETs demonstrate a dominant photovoltaic effect (a shift in V_{TH}) under visible light illumination more pronounced with blue light due to its higher intensity. However, under UV irradiation, photo-OFETs show a combination of photoconductive (an increase in the drain current) and photo-voltaic effect. Photo-induced shift in V_{TH} under visible illumination was found to increase with increasing illumination intensity, illumination time, and applied gate bias during illumination, and it was saturated upon increase in illumination time with characteristic trapping time of 59 s. A Higher exposure time under UV irradiation led to a positive shift in threshold voltage and reduction in the saturation current and mobility. On increasing the gate bias during irradiation, similar positive shift in V_{TH} and reduction in mobility values was observed. These photo-OFETs showed a fast dynamic response to periodic illumination pulses of visible and UV lights, displaying their ability to function as photo-controlled switches. A high drain current modulation (ratio of currents under illuminated and dark conditions) with maximum of 10^5 was achieved for blue colored illumination with a small intensity of 1.7 mW/cm^2. For green light, photo-responsivity of 35mA/W was obtained at a small light intensity of 0.4 mW/cm^2. Under UV irradiation, OFETs yielded a maximum drain current modulation of ~500, a maximum photo-responsivity of ~43 mA/W, and a maximum detectivity of 6.9×10^8 cm $Hz^{0.5}/W$ at an intensity of 1.8 mW/cm^2.

7.2 ORGANIC SEMICONDUCTORS UNDER ILLUMINATION

When an organic semiconductor is illuminated with light, photons are absorbed and a neutral excited state termed exciton, which is a bound electron-hole pair, is generated [Kippelen and Bredas, 2009]. These excitons have larger binding energy in comparison to inorganic semiconductors, of the order of a few hundreds of meV. The magnitude of exciton binding energy is larger due to low dielectric constant, electron-electron correlation and electron-phonon coupling phenomena typical to the π -conjugated compounds. Contrary to inorganic semiconductors, due to larger binding energy, excitons in organic semiconductors are unable to dissociate spontaneously into free electron-hole pairs. As the exciton binding energy is relatively larger, there is a considerable potential barrier for an excitonic state to convert into the charge pair state. However, this barrier may be reduced and generation of free electron-hole pairs (photo-generation) can be enhanced by application of an external electric field. However, an exciton may undergo other phenomena before dissociation, which include radiative decay, exciton diffusion and exciton quenching. Exciton diffusion includes hopping of excitons through Förster mechanism. Diffusion length are tedious to predict and are material specific. Typical exciton diffusion lengths are ~10 nm. A high degree of photo-generation requires the exciton generation within the diffusion length. Exciton quenching can also take place through several paths including non-radiative decay, charge annihilation and intersystem crossing [Baeg *et al.*, 2013].

When an organic semiconductor is excited by absorption of a photon, one electron is excited from HOMO to LUMO and organic molecule in its ground state is excited to a singlet exciton state (net spin of zero). Figure 7.1 depicts possible transitions between electronic states of an

isolated molecule. The transition 2 represents a radiative decay and results in the emission of light and is called fluorescence. Triplet excited state T1 (net spin of one) is generated from an intersystem crossing (transition 4). The radiative transition 6 (Triplet excited state to ground state) is called phosphorescence. The transitions 3 and 5 from higher singlet state to the ground state are non-radiative. Finally transition 7 is the absorption of a photon that brings state T1 to higher triplet excited states Tn. Singlet relaxation may cause branching from excitonic state to charge pair state (Transition 8). Singlet relaxation may also result in the population of vibrationally hot S1 states, which can overcome the barrier and split into free charge carriers (Transition 9 → Transition 10) [Baeg *et al.*, 2013, Scheblykin *et al.*, 2007, Mikhnenko *et al.*, 2015].

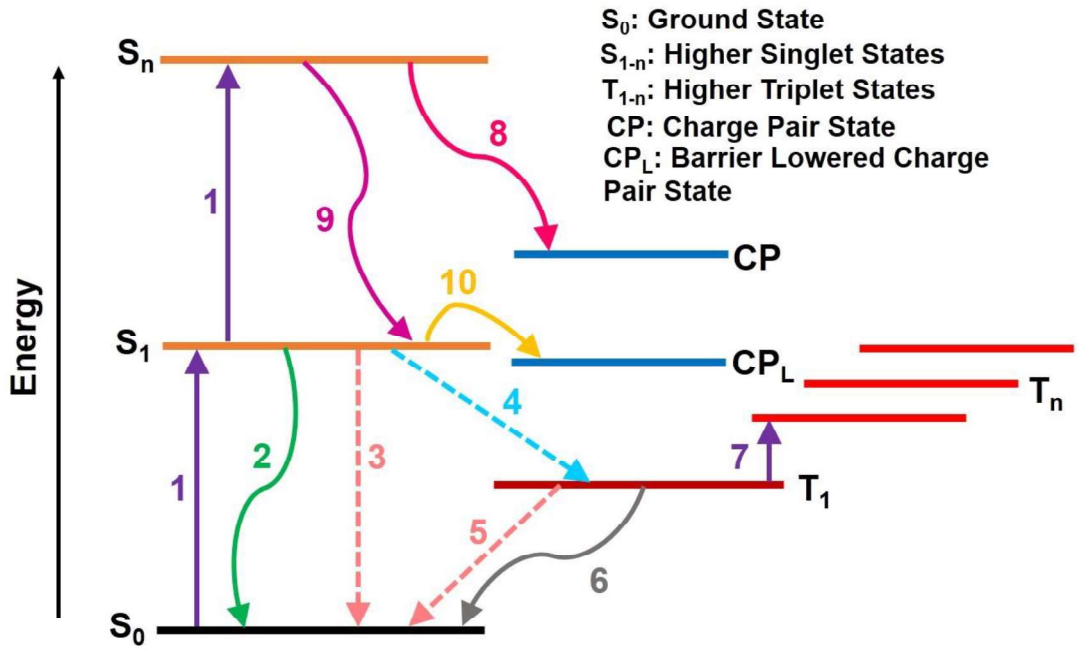

Figure 7.1: Electronic transitions in an organic semiconductor. Photon absorption (1); Photo-induced absorption (7); Radiative transitions: fluorescence (2), Phosphorescence (6); Intersystem crossing (4); Non-radiative transitions (3, 5); CP state generation by branching (8); CP_L state generation by relaxation and vibrational energy (9→10).

7.3 OPERATION OF PHOTO-OFETs

In a normal OFET, in accumulation region and a particular drain bias (V_{DS}), amount of drain current flowing through transistor channel is governed by the magnitude of gate voltage (V_{GS}). Interestingly, in photo-OFETs the channel conductance can be additionally controlled by absorption of light. Light illumination on the channel of the photo-OFETs may induce two types of typical effects. Photovoltaic effect is dominantly observed when the transistor is operated in the accumulation region, whereas the photoconductive effect prevails when the device operates in the depletion region.

7.3.1 Photovoltaic Mode

In a p-channel photo-OFET, free charge carriers are generated on photo-generated exciton dissociation. The photo-generated holes easily flow towards the drain electrode due to their high mobility, whereas electrons get trapped at the dielectric-semiconductor interface where they lower the hole injection barrier between the source and the semiconductor channel. This barrier lowering brings a positive shift of V_{TH}. The photocurrent caused by the photovoltaic effect can be expressed as following [Choi *et al.*, 2003, Kang *et al.*, 2004],

$$I_{ph,pv} = g_m \Delta V_{TH} = \frac{AkT}{q} \ln\left(1 + \frac{\eta q \lambda P_{opt}}{I_{pd} hc}\right) \qquad (7.1)$$

where η is the photo-generation quantum efficiency, P_{opt} is the incident optical power, I_{pd} is the dark current for minority charges, hc/λ is the photon energy, g_m is the transconductance, ΔV_{TH} is the threshold voltage shift, and A is a proportionality parameter [Wakayama *et al.*, 2014].

7.3.2 Photoconductive Mode

When the OFET is in the depletion mode (off state), the photo-generated I_{DS} increases linearly with the incident optical power, due to a photoconductive effect. The current can be modeled according to following equation [Sze and Ng, 2006]:

$$I_{ph,pc} = \left(q\mu_p pE\right)WD = BP_{opt} \qquad (7.2)$$

where μ_p is the mobility of majority charge carriers, p the charge concentration, E the electric field in the channel, W the gate width, D the depth of absorption region, and B is a proportionality factor.

7.3.3 Figures of Merit of a photo-OFET

The figures of merit of a photo-transistor, the current modulation or the ratio of photo and dark current (P), and photo responsivity (R) were calculated using following equations,

$$P = \frac{I_{photo} - I_{dark}}{I_{dark}} \qquad (7.3)$$

$$R = \frac{I_{photo} - I_{dark}}{AP_i} \qquad (7.4)$$

where I_{photo} and I_{dark} are the currents under illuminated and dark conditions, A is the effective device area and P_i is the power of the incident illumination per unit area [Chou *et al.*, 2014].

7.4 EXPERIMENTATION

Neat TIPS-pentacene OFETs with HfO_2-PVP bi-layer gate dielectric were fabricated in bottom-gate top-contact architecture on flexible PET substrate, having a 130 nm thick layer of ITO. Fabrication procedure has been described earlier in chapter 5. Capacitance density (C_i) of the HfO_2/PVP hybrid dielectric layer was obtained from parallel plate capacitors and found to be 24.46±0.71 nF/cm² at 1 KHz.

To study the steady-state photo-response of the devices under visible illumination of different colors, a 4 terminal, low power LED lamp was used as a light source, capable of emitting uniform light of different colors on different terminals (red : λ_{min} ~ 620 nm, green : λ_{min} ~ 520 nm, and blue : λ_{min} ~ 460 nm). The light source was adjusted to shine right above the sample with maximum intensities of 0.3 mW/cm², 0.4 mW/cm² and 1.7 mW/cm² for red, green and blue lights respectively. To investigate photo-response of the devices to UV irradiation, a 2 terminal low power UV LED with a peak wavelength of 365 nm was used as a UV light source. This light source was adjusted to shine above the sample with maximum intensity of 1.8 mW/cm².

7.5 RESULTS & DISCUSSIONS

Figure 7.2 shows the UV and visible absorption spectrum of TIPS-pentacene. A higher absorbance can be noticed in the near UV region as compared to visible portion. In the visible region, relatively higher absorbance can be observed in the red region of the spectrum. If the photo-responsivity of the organic semiconductor follows the absorption spectrum, photo-response will be symbatic. In case of disagreement between photo-responsivity and absorption spectrum, photo-response will be antibatic [Harrison *et al.*, 1997, Köhler and Bässler, 2015].

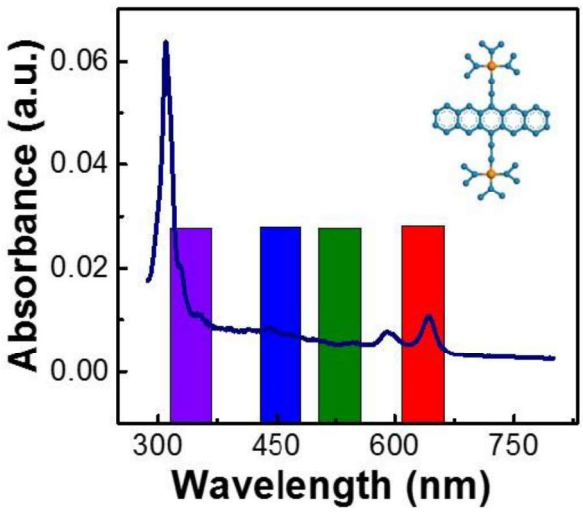

Figure 7.2: UV and visible absorption spectrum of TIPS-pentacene.

7.5.1 Visible Photo-response

Figure 7.3 shows the photo-response of another representative device under illumination with visible lights of different minimum wavelengths: red (λ_{min} ~ 620 nm), green (λ_{min} ~ 520 nm) and blue (λ_{min} ~ 460 nm) with varying luminous intensities for each wavelength on linear and logarithmic scales. These transfer characteristics were measured instantaneously after turning the illumination ON, with illumination ON throughout the measurement. The photo-response was dominated by photovoltaic effect (shift in V_{TH}), rather than photoconductive effect (increase in off current). On illumination, excitons are generated in the TIPS-pentacene layer, which eventually dissociate into free electrons and holes. More mobile charge carriers (holes) move readily towards drain terminal and cause rise in drain current whereas the less mobile electrons are trapped on the PVP interface which has the high density of hydroxyl (-OH) groups. These trapped electrons effectively reduce the potential barrier between source and channel, which ultimately results into a decrease in V_{TH} [Dutta and Narayan, 2004, Mas-Torrent *et al.*, 2006]. This can be observed from the figures that on illumination, transfer curve shifts towards positive gate voltages (reduction in V_{TH}), with higher shift with increasing intensities. Overall V_{TH} shift is the highest for blue illumination due to higher intensity of blue illumination. The photo-response of the device is prominent around V_{TH} (onset of accumulation) because of the abundance of photo-generated charge carriers over scarce field-generated carriers near and below V_{TH}. At higher V_{GS} values, photo-response is subdued due to excess of field-induced charge carriers.

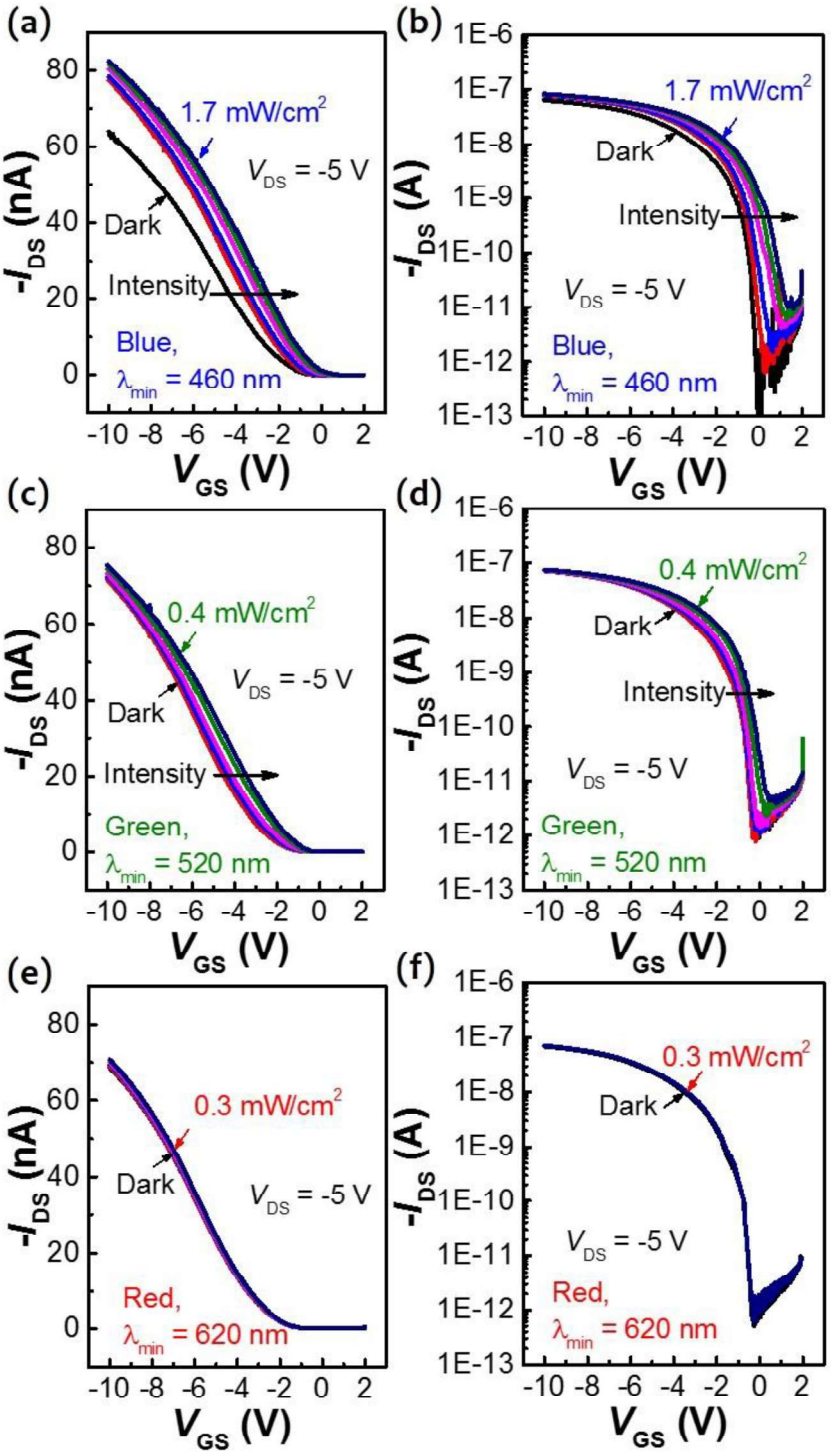

Figure 7.3: Transfer characteristics of TIPS-pentacene OFET on linear and logarithmic scales respectively for blue **(a) & (b),** green **(c) & (d),** and red illumination **(e) & (f),** with varying intensity.

From the transfer curves of the representative device given in Figure 7.3, values of P and R for blue, green and red lights are extracted. Figure 7.4(a) shows the variation of P as a function of gate voltage at a fixed drain voltage. Maximum P value for blue, green and red lights were found to be ~4×10^4, ~100 and ~40 respectively. High P was achieved at low operating voltages, close to V_{TH} of the pristine and unilluminated device. For a device under illumination, the drain current is the sum of the currents due to field-generated carriers and photo-induced carriers. As discussed earlier, below V_{TH}, the photo generated current is the

major portion of the drain current, whereas at higher gate voltages, field-generated current is predominant [Chou *et al.*, 2014, Dutta and Narayan, 2004, Mas-Torrent *et al.*, 2006]. This causes the maximum change in drain current and hence the highest P value in the proximity of V_{TH} of the pristine device. Current gain is reduced to unity at more negative gate voltages due to comparable number of photo-generated and field-generated charge carriers. At higher positive gate voltages, P is reduced due to almost equal levels of off currents in dark and illuminated conditions. Figure 7.4(b) shows the variation in R as a function of gate voltage. At positive gate voltages, R is very small due to smaller magnitude of change in drain current. However, value of R increases with increasing gate voltages (in negative direction) due to rising magnitude of change in drain current, which saturates at higher gate voltages due to comparable levels of field-generated and photo-generated currents. Maximum R of the representative device for blue, green and red lights were 17 mA/W, 35 mA/W and 11 mA/W respectively with light intensities ranging from 1.7 to 0.3 mW/cm², which is slightly lower than that for high voltage operated TIPS-pentacene photo-OFETs on rigid substrates demonstrated at high illumination intensities of the incident light [Gunduz and Yakuphanoglu, 2012].

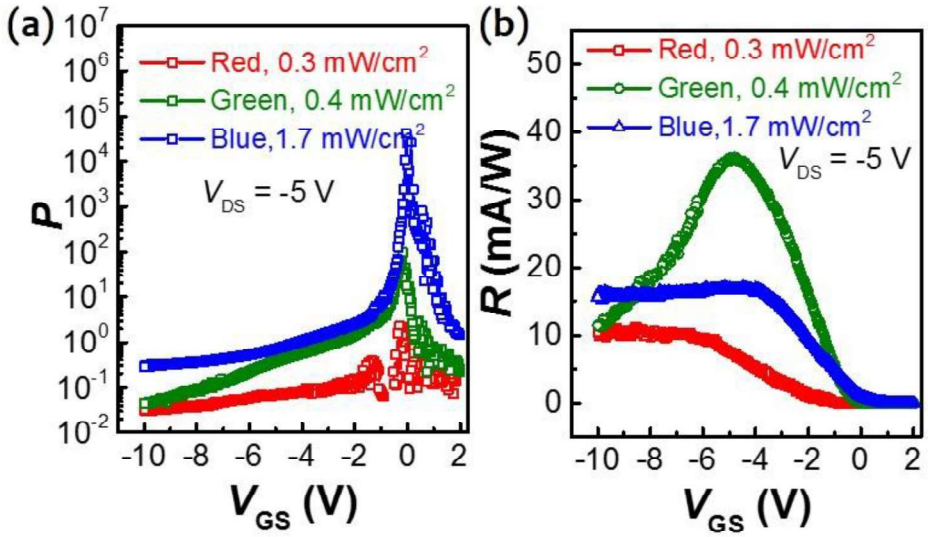

Figure 7.4: Variation in current modulation **(a),** and photo-responsivity **(b),** with applied gate voltage for various illuminations.

In addition, external quantum efficiency (EQE) was calculated which is the ratio of photo-generated carriers increasing the drain current to the number of incident photons in the channel area [Yu *et al.*, 2013]. EQE can be expressed mathematically as following,

$$EQE = \frac{\left(I_{\text{photo}} - I_{\text{dark}}\right)hc}{eP_{\text{i}}A\lambda_{\text{peak}}} = \frac{Rhc}{e\lambda_{\text{peak}}} \qquad (7.5)$$

EQE corresponding to maximum responsivities values were found to have value of 4.6 %, 8.3 % and 2.2 % for blue, green and red illumination. This indicates that larger number of photo-induced carriers are generated per incident photon of green light illumination, which explains higher sensitivity of photo-OFETs to green light illumination. The photosensitivity of photo-OFETs do not follow the absorption spectrum in Figure 7.2, suggesting an antibatic behavior [Harrison *et al.*, 1997, Köhler and Bässler, 2015]. In this case, when absorption coefficient is higher, light is mostly absorbed in the top layers of the semiconductor (when light is shined from top), producing excitons mainly in these top layers. However, these excitons are unable to contribute to the photocurrent of the device due to their short diffusion lengths. In contrast, when the absorption coefficient is small, excitons are also generated in the bulk and near the dielectric-semiconductor interface. Excitons which are generated in the vicinity of

interface (distance shorter than diffusion length), can reach to interface, and contribute towards photo-induced effects [Harrison *et al.*, 1997, Köhler and Bässler, 2015].

Figure 7.5 shows the illumination time dependence of the photo-response. In Figure 7.5(a), the transfer characteristics of photo-OFET is shown which were measured in dark conditions after illuminating the device for a particular integration time and at constant biasing conditions (V_{GS} = 10 V, V_{DS} = 0 V). It is to be noted that drain bias was not applied during illumination in order to achieve a homogenous field distribution. Providing a gate bias during illumination has a profound effect on the photo-response as it can attract or repel majority charge carriers. Figure 7.5(a) shows that with increasing illumination time, transfer curve shifts to more positive V_{GS}, indicating increasing shift in V_{TH}. A higher illumination time causes higher degree of exciton generation and charge trapping, which ultimately results in a higher reduction in V_{TH} (shifting towards more positive V_{GS}).

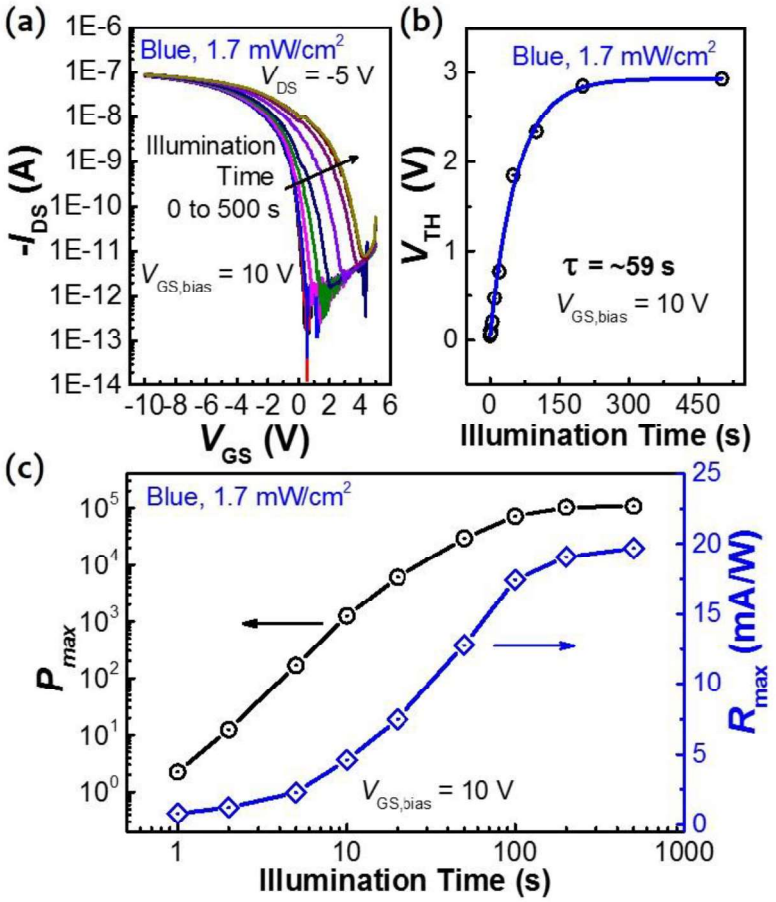

Figure 7.5: (a) Effect of illumination time with constant biasing conditions ($V_{GS,bias}$ = 10 V, $V_{DS,bias}$ = 0 V) on the photo-response. **(b)** Exponential variation of V_{TH} with illumination time. **(c)** Dependence of maximum current modulation and photoresponsivity on illumination time.

Figure 7.5(b) shows the variation of V_{TH} as a function of illumination time. V_{TH} increases linearly with illumination time, however saturates at larger values of integration times. Qualitatively, V_{TH} under illumination can be expressed as an exponential function of illumination time as given below,

$$V_{TH}\left(t_{int}\right) = \Delta V_{TH,sat} \exp\left(-\frac{t_{int}}{\tau}\right) + V_{TH,sat} \qquad (7.6),$$

where $\Delta V_{TH,sat}$ is the difference in the threshold voltages of the dark and final saturated conditions, τ is the characteristic trapping time and $V_{TH,sat}$ is the final threshold voltage of the saturated condition. This expression suggests that the whole V_{TH} shift mechanism is limited by

charge trapping. However, it should be noted that the increase in drain current and related V_{TH} shift is not always trapping limited but at smaller integration times, it may be optically absorption limited [Milvich *et al.*, 2015]. By an exponential fit as per equation, a characteristic trapping time of ~59 s was extracted for blue light illumination, which is lesser than a previous report, signifying a faster response [Milvich *et al.*, 2015]. Figure 7.5(c) shows the variation of P_{max} and R_{max} of the representative device with illumination time, which can be observed to rise with increasing illumination time due to increasing magnitude of photo-currents. Highest values of P_{max} and R_{max} were found to be 1.07×10^5 and ~20 mA/W respectively for an illumination time of 500 s with constant biasing conditions of V_{GS} = 10 V and V_{DS} = 0 V in this case. This current modulation of 10^5 achieved from a low voltage flexible TIPS-pentacene device at small light intensity is comparable to that reported for TIPS-pentacene photo-OFETs on rigid substrates with high light intensity and high operating voltages [Kim *et al.*, 2010]. It should be noted that application of gate bias during illumination yields improved values of P_{max} and R_{max} in contrast to the earlier case where no gate bias was applied. This improvement indicates that photo-response of a photo-FET can be enhanced by application of a suitable gate bias during illumination [Kim *et al.*, 2014].

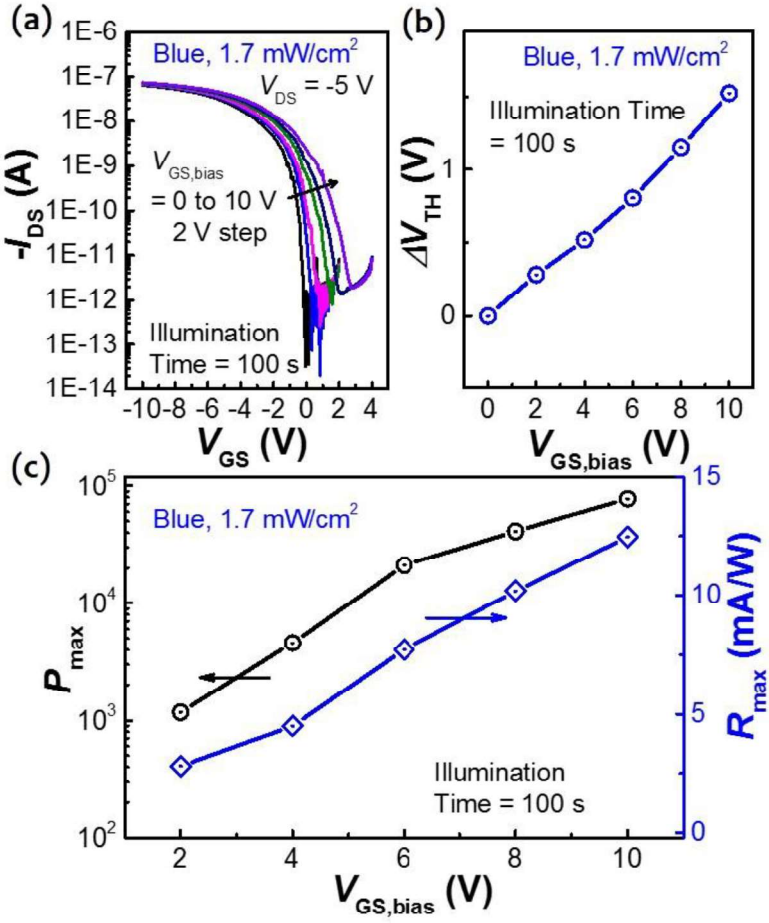

Figure 7.6: (a) Effect of gate bias during illumination on the photo-response of an OFET for constant illumination time of 100 s. **(b)** Linear dependence of shift in V_{TH} on the applied gate bias during illumination. **(c)** Variation of maximum current modulation and photo-responsivity with the applied gate bias during illumination.

Figure 7.6(a) shows the transfer characteristics of the photo-OFET with different gate biases applied during illumination for a fixed illumination time of 100 s. With increasing $V_{GS,bias}$ during illumination, transfer curve shifts towards more positive gate voltages, leading to a V_{TH} shift. This V_{TH} shift increases with $V_{GS,bias}$ due to higher degree of electron trapping at higher

$V_{GS,bias}$. Figure 7.6(b) shows the dependence of V_{TH} shift on $V_{GS,bias}$. V_{TH} shift vary in proportion to the applied $V_{GS,bias}$, indicating a linear relationship between both parameters. Figure 7.6(c) shows the variation in P_{max} and R_{max} of the representative device with applied gate bias during illumination for a fixed illumination time of 100 s. P_{max} and R_{max} increase monotonically with applied gate bias, which can be associated with higher levels of photo-current at higher gate bias.

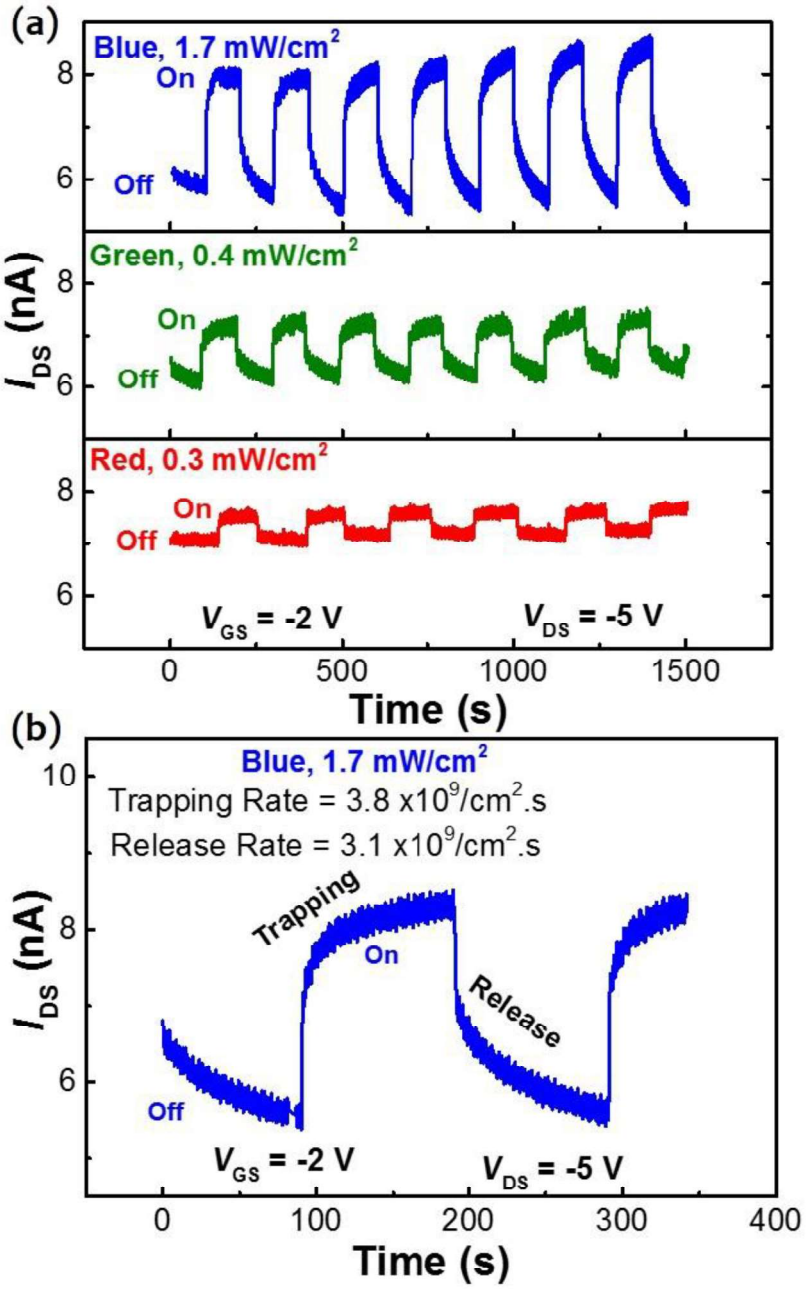

Figure 7.7: (a) Dynamic response of TIPS-pentacene photo-OFET for different illuminations. **(b)** Illustration of drain current response for a single cycle of blue light illumination. Trapping and release rates were extracted from the initial 30 s of the ON and OFF regions.

Figure 7.7(a) shows the dynamic response of another photo-OFET under illumination with different color lights. Under this investigation, devices were subjected to periodic illumination pulses for 100 s, and the drain current was measured at V_{GS} = -2 V, V_{DS} = -5 V in the interval of 0.5 s. With these illumination pulses, a fast switching phenomenon was observed.

Maximum response was obtained for blue light irradiation, due to its higher illumination intensity. The magnitude of change in the drain current on illumination is subsequently lesser for green and red light illumination. Lesser variation in drain current can be attributed to their lower intensities. With turning the illumination on, in the initial stages, drain current rises quickly due to quick collection of photo-generated holes at the drain terminal, whereas the photo-generated free electrons, get trapped on the hydroxyl group rich PVP surface, whereas at later stages, rate of rise in the drain current slows down due to coulombic repulsion between trapped and incoming electrons [Kim *et al.*, 2014]. On terminating the illumination, drain current reduces quickly. However, it does not reach instantly to its initial level under dark conditions, and some persistent photoconductivity is remained. The initial sudden reduction in the drain current after terminating the illumination is due to faster recombination of proximal charge carriers, whereas the metastable state, identified by a slow decay in drain current is due to poor recombination process as a consequence of increased spatial distance between charge carriers to be recombined [Dutta and Narayan, 2004, Mas-Torrent *et al.*, 2006].

Figure 7.7(b) shows the drain current response to a single cycle of a periodic blue light pulse. It can be observed from the figure that rates of change in drain current are different on turning the illumination on and off respectively, indicating a different trapping and releasing behavior of charge carriers [Kim *et al.*, 2014]. Quantitatively, these rates can be calculated using following expression [Yu *et al.*, 2013],

$$Rate = \frac{dQ}{dt} = C\frac{d\left(V_{TH}\right)}{dt} = -\left(\frac{2LC}{\mu_{sat}W}\right)^{1/2}\frac{d\left[\left(I_{DS}(t)\right)^{1/2}\right]}{dt} \qquad (7.7)$$

where Q is the charge density. This equation describes temporal behavior of the excess photo-generated charge carrier density. To estimate the trapping and release rates, the linear fit was applied on $\{I_{DS}(t)\}^{1/2}$ in the initial 30 s of the regions indicated by trapping and releasing in Figure 7.7(b), and slope was extracted [Kim *et al.*, 2014]. Various rates calculated from a representative device for all three illuminations are given in Table 7.1. From the table it can be noticed that trapping and release rates are highest for blue irradiation; 3.8×10^{9} cm^{-2} s^{-1} and 3.1×10^{9} cm^{-2} s^{-1} respectively, as compared to all other rates for green and red light illumination due to higher intensity of blue light irradiation. Interestingly, it can also be observed that off currents in all cases to reach dark current levels without applying a de-trap bias, a phenomenon which is rarely observed.

Table 7.1: Summary of various trapping and release rates.

Illumination	Trapping (10^9 cm^{-2} s^{-1})	Release (10^9 cm^{-2} s^{-1})
Red (0.3 mW/cm²)	0.22	0.24
Green (0.6 mW/cm²)	0.54	0.39
Blue (1.7 mW/cm²)	3.76	3.10

Table 7.2: Summary of various studies based on photo-OFETs.

OSC	Proc.	Substrate	Dielectric	Op. Vol. (V)	I (mW/cm²)	R_{max} (A/W)	P_{max}	λ (nm)/ Color	Ref.
Pentacene	V	R (n-Si)	SiO_2	50	9.5	1	9×10^3	650	[Noh and Kim, 2007]
P3HT	S	R (n-Si)	SiO_2	75	51	16	3.8×10^3	White	[Tanusri *et al.*, 2010]
Pentacene	V	R	SiO_2/ PMMA	-	≤0.6	92	-	465/ Blue	[Zan *et al.*, 2010]
TIPS-pentacene	S	R (glass)	PVP	40	13	-	~10^7	White	[Kim *et al.*, 2010]
TIPS-pentacene	S	R (n-Si)	SiO_2	20	80	53.5×10^{-3}	-	White	[Gunduz and Yakuphanoglu, 2012]
PdPC	V	R (n-Si)	SiO_2	50	100	7.61×10^{-4}	1.4×10^3	655	[Peng *et al.*, 2013]
PBDFT-DTBT	S	R (p-Si)	SiO_2	40-50	100	0.36	1.2×10^5	White	[Huang *et al.*, 2014]
PTCDI-C13H27	V	F (PES)	PVP	6-18	22.5	0.41	4×10^4	532	[Chou *et al.*, 2014]
MDMO-PPV	S	R (Glass)	PMMA	80	17	0.12×10^{-3}	1.24×10^2	White	[Kösemen *et al.*, 2016]
DNTT	V	R (Si)	PLA	60	80	-	~10^4	White	[Chu *et al.*, 2016]
TIPS-pentacene	S	F (PET)	HfO_2/PVP	5-10	1.7	2.0×10^{-2}	1.07×10^5	460/ Blue	2016, This work

Table 7.2 presents a comparative summary of various studies based on organic photo-transistors. It can be observed from the table that in most of the reports, photo-OFETs have been fabricated on rigid substrates like glass and silicon. Many of these operate at high voltages ranging from 20 V to 80 V except a few including [Chou *et al.*, 2014]. A higher photo-responsivity in [Noh and Kim, 2007, Tansuri *et al.*, 2010] have been obtained at cost of 10 to 12 times higher operating voltages (drain voltage) than that of our study. Additionally, this work demonstrates higher current modulation of 10^5 with small illumination intensity (I) of 1.7 mW/cm² at lower operating voltages of 5 V, whereas other studies report lower or similar values, however, with much higher (5.5 to ~60 times) illumination intensity and higher operating voltages ranging from 40 to 80 V. In overall, this work demonstrates high P_{max} values in flexible solution processed photo-OFETs at much smaller illumination intensity with moderate intensity independent R_{max}, while operating at lower voltages.

7.5.2 UV Photo-response

Figure 7.8 shows the effect of UV irradiation on the transfer characteristics of a representative device on logarithmic and linear scales. The UV irradiation induces a combination of photo-conductive (an increase in the drain current) and photo-voltaic effect (a shift in V_{TH}). UV photons incident on semiconductor film cause exciton generation, which eventually dissociate into free electrons and holes, as earlier discussed in section 7.5.1. Since holes have higher mobility in a p-type semiconductor, they escape swiftly towards the drain electrode increasing the levels of drain current. Less mobile electrons are trapped on PVP/TIPS-pentacene interface, finally leading to reduced V_{TH} [Dutta and Narayan, 2004, Mas-Torrent *et al.*, 2006].

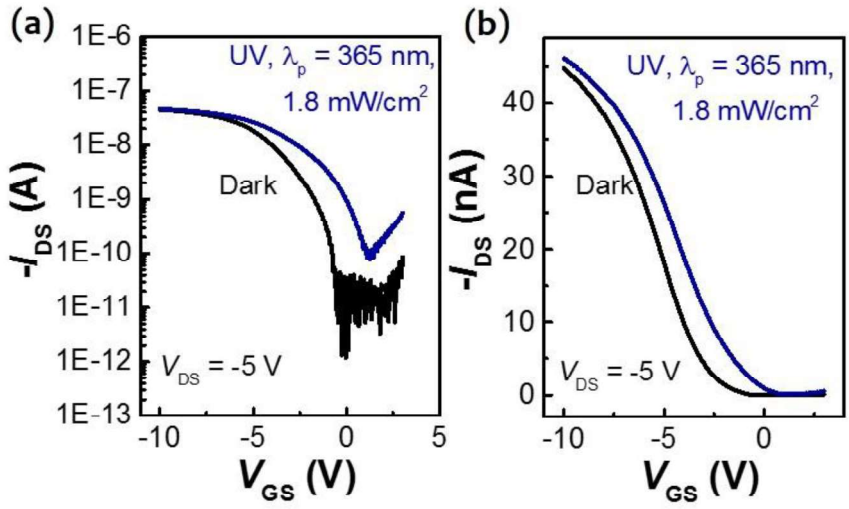

Figure 7.8: Transfer characteristics of TIPS-pentacene OFET on logarithmic **(a),** and linear scales **(b),** under UV irradiation.

Table 7.3 lists device parameters for a set of five devices undergone UV irradiation. It can be observed from the table that average mobility of OFETs is reduced, whereas the average threshold voltage has been shifted towards positive voltages after UV exposure. Figures of merit of photo-transistors; current modulation and photo-responsivity have been calculated using Equation (7.3) and Equation (7.4). Another performance parameter of detectivity has been calculated using following expression,

$$D^* = \frac{R\sqrt{A}}{\sqrt{2eI_{dark}}} = \frac{R}{\sqrt{2eJ_{dark}}} \qquad (7.8)$$

where R is the photo-responsivity of the device, J_{dark} is corresponding dark current density and e is the electronic charge [Baeg *et al.*, 2013]. Maximum values of photo-responsivity (R_{max}), current modulation (P_{max}) and detectivity (D^*_{max}) of ~43 mA/W, ~500 and 6.9×10^8 cm $Hz^{0.5}$/W were obtained respectively for an intensity of 1.8 mW/cm^2 of UV illumination at V_{DS} = -5 V, from a set of 5 devices. It is to be noted that the above performance has been obtained with solution processed flexible photo-transistors while operating at lower voltages, which is comparable to some of the previously reported diode UV detectors based on organic and/or hybrid materials [Li *et al.*, 2005, Chen *et al.*, 2006, Si *et al.*, 2007, Ray and Narasimhan, 2007, Zhang *et al.*, 2010, Li *et al.*, 2011].

Table 7.3: Summary of electrical parameters for a set of 5 devices undergone UV irradiation.

Mobility ($cm^2 V^{-1} s^{-1}$)		Threshold Voltage (V)		P_{max}	R_{max} (mA/W)	D^*_{max} (cm $Hz^{0.5}$/W)
Before	After	Before	After			
0.031±0.009	0.019±0.006	-0.63±0.48	1.24±0.68	~500	~43	6.9×10^8

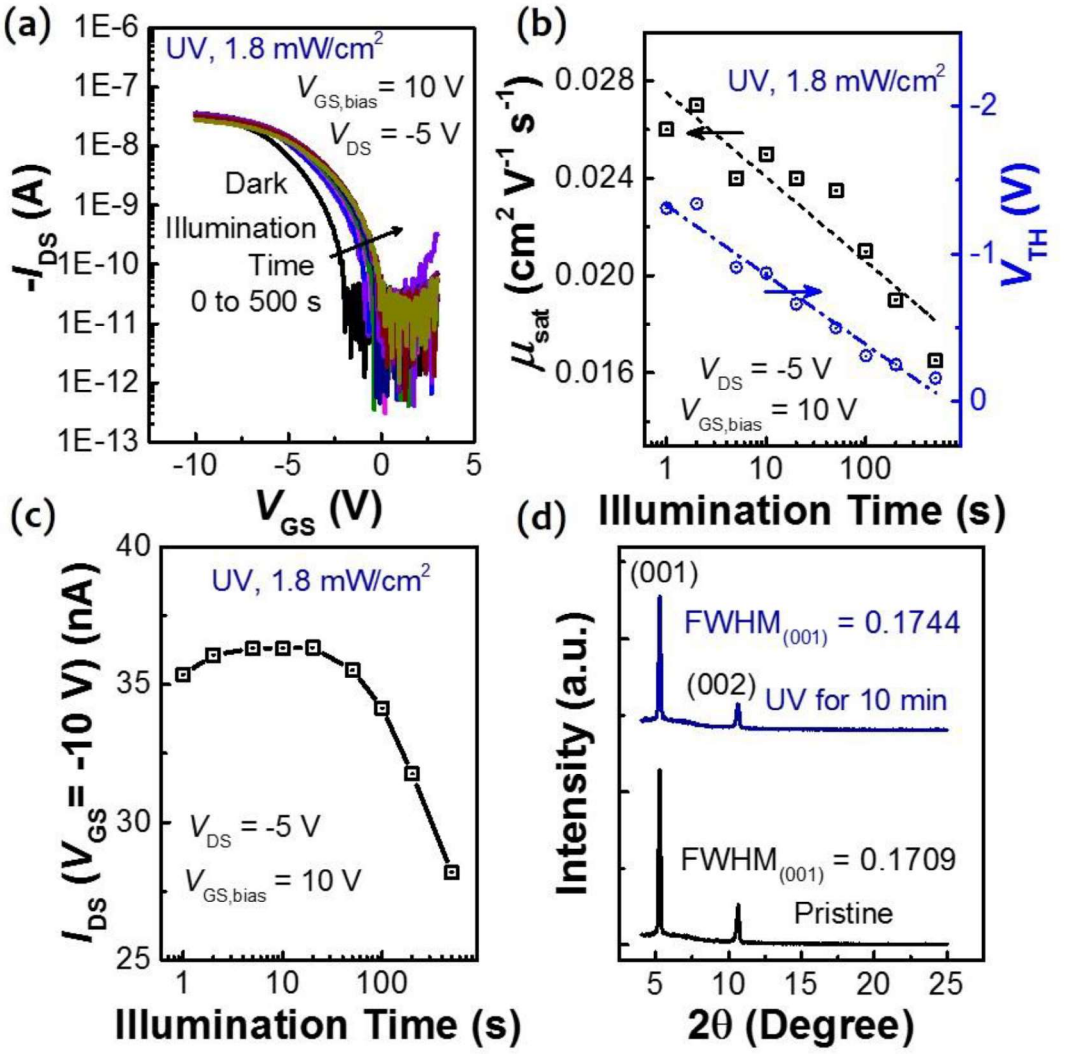

Figure 7.9: (a) Effect of UV illumination time on the transfer characteristics of the OFET. **(b)** Variation of μ_{sat} and V_{TH} with increasing illumination time. **(c)** Trend of maximum drain current at V_{GS} = -10 V with increasing illumination time. **(d)** X-ray diffractogram of a pristine and 10 minute UV irradiated sample.

Figure 7.9(a) shows the effect of increasing irradiation time on the transfer characteristics of representative OFET which were measured in dark conditions after illuminating the device with UV irradiation for a particular irradiation time and at constant biasing conditions of V_{GS} = 10 V. It can be observed that with increasing illumination time, transfer curves shift towards positive values of V_{GS}, ultimately resulting in a shift in V_{TH}. This shift in V_{TH} can be attributed to the increased exciton generation and charge trapping under increasing illumination time. Figure 7.9(b) shows the variation in μ_{sat} and V_{TH} as a function of illumination time. With increasing illumination time, μ_{sat} follows a decreasing trend, while V_{TH} increases linearly towards positive voltages. Not only the μ_{sat} and V_{TH}, the magnitude of drain current in saturation regime also varies with UV illumination time. Variation in maximum drain current at V_{GS} = -10 V is plotted with UV illumination time and shown in Figure 7.9(c). Drain current shows a little increment at smaller illumination time after which it rapidly falls at higher illumination time. At smaller values of illumination time, the photoconductive effect is prevalent which causes a small increment in the drain current. To ascertain the reason of current roll-off at higher values of illumination time, X-ray diffraction studies were performed. Figure 7.9(d) shows the X-ray diffractogram of a pristine and 10 minute UV irradiated sample. A slight increase in FWHM was observed on UV irradiation signifying a decrease in crystallinity. The crystallinity was reduced due to destructive nature of prolonged UV

irradiation, which has tendency to break the bonds in crystals and generate defects. Another reason for the impaired conduction can be the UV induced photo-chemical degradation of the organic semiconductor which is further enhanced in the presence of oxygen and moisture. This degradation can also generate defects in semiconductor layer [Goldmann *et al.*, 2006, Gu and Kane, 2008, Wrachien *et al.*, 2011]. Hence increased number of defects sites and decreased crystallinity due to prolonged UV exposure lead to deteriorated quality of charge transport and therefore decreased drain current and charge carrier mobility.

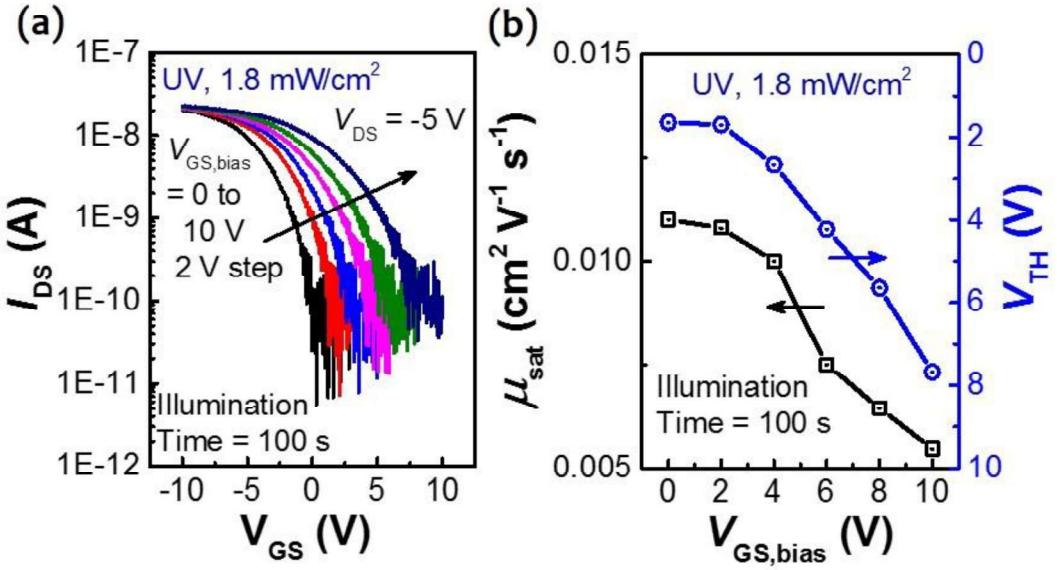

Figure 7.10: (a) Effect of increasing gate bias during illumination on the transfer characteristics of an OFET for a constant illumination time of 100 s. **(b)** Dependence of μ_{sat} and shift in V_{TH} on the applied gate bias during illumination.

Figure 7.10(a) shows the effect of applied gate bias during UV illumination on the transfer characteristics of the OFET for a constant illumination time of 100 s. An increasing $V_{GS,bias}$ during illumination causes a shift in the transfer curve towards positive gate voltages, resulting in a positive V_{TH} shift. Figure 7.10(b) shows the variation in μ_{sat} and V_{TH} as a function of $V_{GS,bias}$. μ_{sat} decreases whereas V_{TH} shifts to positive values in proportion to the applied $V_{GS,bias}$. A higher positive $V_{GS,bias}$ causes higher degree of electron trapping, which results in larger V_{TH} shift. However, decrease in the mobility may be ascribed to the deteriorated quality of charge transport under cumulative effect of UV irradiation as discussed earlier.

Figure 7.11(a) shows the dynamic response of the OFETs under UV illumination. Under this study, the devices were irradiated with periodic UV illumination pulses (ON and OFF period = 20 s), and the drain current was measured at V_{GS} = -5 V, V_{DS} = -5 V in the interval of 0.5 s. A rapid switching phenomenon was observed with these irradiation pulses. On turning on the UV illumination, drain current begins to increase linearly due to photo-generated holes, which reach quickly to drain terminals due to their higher mobility. After turning the illumination off, drain current starts to decrease linearly due to de-trapping of electrons and their recombination with holes. Trapping and release rates during illumination ON and OFF states can be calculated using Eq. (7.7). Figure 7.11(b) shows the plot of $\{I_{DS}(t)\}^{1/2}$ for a single cycle of UV illumination. To estimate the trapping and release rates, the linear fit was applied on $\{I_{DS}(t)\}^{1/2}$ in the ON and OFF regions in Figure 7.11(b), and slope was extracted [Kim *et al.*, 2014]. Trapping and release rates in UV ON and OFF regions were found to have values of 5.7×10^9 cm^{-2} s^{-1} and 12.1×10^9 cm^{-2} s^{-1} respectively. A higher release rate than the trapping rate signifies that de-trapping of electrons is faster in the absence of UV illumination than their trapping at PVP/TIPS-pentacene interface during illumination.

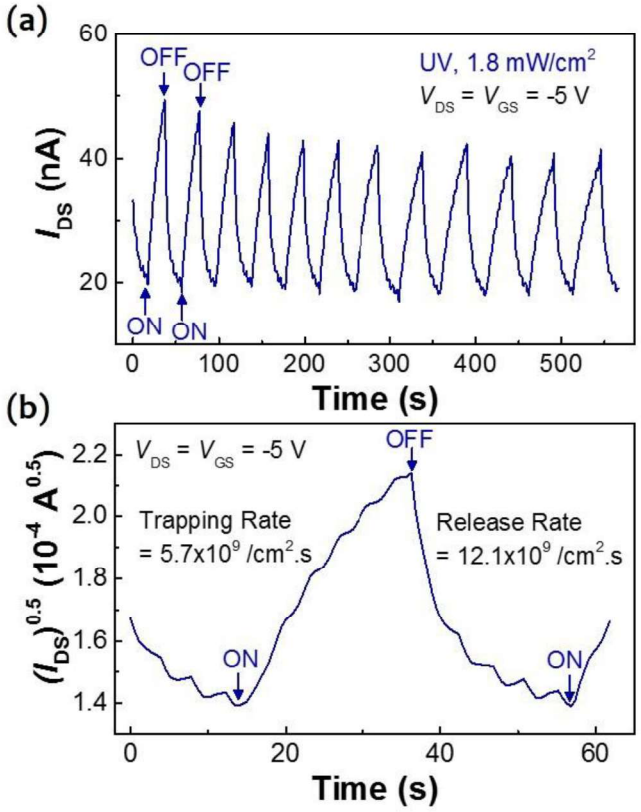

Figure 7.11: (a) UV switching response of TIPS-pentacene OFETs. **(b)** Variation in $\{I_{DS}(t)\}^{1/2}$ for a single cycle of UV illumination. Slopes have been extracted from the linear fit in the ON and OFF regions.

7.6 CONCLUSIONS

Solution processed, flexible photo-OFETs were demonstrated with TIPS-pentacene as the photo-sensitive active layer. An average mobility of 0.11(±0.08) $cm^2\ V^{-1}\ s^{-1}$ with high current on-off ratio of ~10^5 were achieved for pristine OFETs for a moderate operating voltage of -10 V. Photo-response of the devices was measured under illumination with visible light (different minimum wavelengths of 620 nm, 520 nm and 460 nm, corresponding to red, green and blue colors respectively) and UV light (peak wavelength 365 nm). For blue, green and UV light illumination (intensity of 1.7 mW/cm^2, 0.4 mW/cm^2 and 1.8 mW/cm^2 respectively), a maximum current modulation of 4×10^4, 10^2 and 5×10^2 and photo-responsivity of 17 mA/W, 35 mA/W and 43 mA/W were achieved respectively. Photo-OFETs demonstrated a maximum detectivity of 6.9×10^8 cm $Hz^{0.5}/W$ to UV light illumination. Photo-OFETs showed a fast switching response to visible and UV illumination pulses. The photo-response to visible illumination was found to increase with illumination intensity, illumination time and applied gate bias during illumination. A maximum current modulation of 10^5 was demonstrated for 500 s of blue light illumination and with a gate bias of 10 V. However, increasing UV irradiation time resulted in an enhanced positive threshold voltage shift and reduced mobility. The saturation drain current at biasing conditions of V_{GS} = -10 V and V_{DS} = -5 V was found to rise slightly for smaller values of irradiation time, however decreased for higher values of illumination time. Similar trend of positive shifting of V_{TH} and mobility roll-off was observed when gate bias during irradiation was increased.

…